

# Slip Effects on MHD Stagnation Point-Flow and Heat transfer over a Porous Rotating Disk

Navid Freidoonimehr<sup>1</sup>, Mohammad Mehdi Rashidi<sup>2</sup>, Shohel Mahmud<sup>3\*</sup>, Foad Nazari<sup>1</sup>

<sup>1</sup> Young Researchers & Elite Club, Hamedan Branch, Islamic Azad University, Hamedan, Iran

<sup>2</sup> Mechanical Engineering Department, Engineering Faculty of Bu-Ali Sina University, Hamedan, Iran

<sup>3</sup> School of Engineering, University of Guelph, Guelph, Ontario N1G 2W1, Canada

## Abstract

The main concern of present study is to investigate the MHD stagnation flow past a porous rotating disk in the presence of the velocity slip condition. The boundary-layer governing partial differential equations (PDEs) are transformed into highly nonlinear coupled ordinary differential equations (ODEs) consist of the momentum and energy equations using similarity solution. The velocity profiles in radial, tangential and axial directions and temperature distribution are obtained via a semi analytical/numerical method, called Homotopy Analysis Method (HAM). An excellent agreement is observed between some of the obtained results of the current study and those of previously published studies. The influences of physical flow parameters such as magnetic interaction parameter ( $M$ ), slip factor ( $\gamma$ ), rotation strength parameter ( $\omega$ ), and suction parameter ( $W_s$ ) on the all fluid velocity components, temperature distribution as well as the skin friction coefficients and the rate of heat transfer are examined and analyzed. This simulation presents the feasibility of using magnetic rotating disk drives in novel nuclear space propulsion engines.

**Keywords:** Velocity slip; Stagnation flow; Porous rotating disk; MHD flow

---

\* corresponding author (smahmud@uoguelph.ca)

## Nomenclature

$a$	constant parameter
$B$	external uniform magnetic field
$B_0$	constant magnetic flux density
$c_p$	specific heat at constant pressure
$F$	self-similar radial velocity
$G$	self-similar tangential velocity
$H$	self-similar axial velocity
$k$	thermal conductivity
$p$	pressure
$P$	self-similar pressure
$p_0$	stagnation pressure
$r$	radial direction in cylindrical polar coordinates
$T$	fluid temperature
$u$	velocity component in the radial direction
$u_e$	external flow velocity
$v$	velocity component in the tangential direction
$w$	velocity component in the axial direction
$w_0$	uniform suction
$z$	normal direction in cylindrical polar coordinates

## Dimensionless parameters

$M$	magnetic interaction parameter $(\sigma B_0^2 / \rho a)$
$Pr$	Prandtl number $(\mu c_p / k)$

$W_s$  suction parameter ( $w_0/\sqrt{\nu a}$ )

$\omega$  rotation strength parameter ( $\Omega/a$ )

$\gamma$  slip factor ( $[(2-\sigma_v)\xi\sqrt{a/\nu}]/\sigma_v$ )

### *Greek symbols*

$\eta$  a scaled boundary-layer coordinate

$\xi$  mean free path

$\theta$  self-similar temperature

$\mu$  dynamic viscosity

$\nu$  kinematic viscosity

$\rho$  density

$\sigma$  electrical conductivity

$\sigma_v$  tangential momentum accommodation coefficient

$\phi$  tangential direction in cylindrical polar coordinates

$\Omega$  angular velocity of the disk

### *Subscripts*

$w$  condition of the wall

$\infty$  condition of the free stream

## **1. Introduction**

One of the most important fluid mechanics classic problems that attracted many attentions in several industrial and engineering processes such as rotating machinery, lubrication, oceanography and computer storage devices is the problem of flow over a rotating disk. Von Karman [1] was the first one who studied the hydrodynamic flow over an infinite rotating disk. In this study, he introduced his famous appropriate transformations, giving rise to ordinary differential equations that are a reduced form of the governing partial

differential equations. The exact solution results for the heat transfer problem of a rotating disk with fluid flow around it were demonstrated by Shevchuk and Buschmann [2]. Attia [3] presented the laminar steady flow of an incompressible viscous fluid past a rotating disk with an infinite expansion in the porous medium. Osalusi *et al* [4] demonstrated the effects of ohmic heating, viscous dissipation, and Hall effect in an MHD flow over the porous rotating disk considering variable fluid properties such as density, viscosity, and thermal conductivity. Beside the theoretical investigations, significant researches have been executed in the field of experimental studies of rotating disk systems [5]. In another study, Asghar *et al* [6] discussed steady 3D flow and heat transfer of viscous fluid on a rotating disk stretching in radial direction. Their results showed that the exact analytical solutions were existed for the case of pure stretching.

No-slip boundary conditions (the assumption that a liquid adheres to a solid boundary) is applied in most of the studies. In some investigations like emulsions, suspensions, foams and polymer solution [7], the no-slip conditions are not adequate. For the slip flow regimes, the standard Navier–Stokes and energy equations can be still applied by taking into account the velocity slip conditions. The slip-flow regimes have been widely studied and the researchers have been concentrating on the analysis of micro-scale in micro-electro-mechanical systems (MEMS) associated with the embodiment of velocity slip condition. Sparrow *et al* [8] assumed the fluid flow due to the rotation of a porous surface disk and employed a set of linear slip flow conditions. As a result of slip condition, a substantial reduction in torque occurred. Sahoo [9] investigated the effect of partial slip, viscous dissipation, and Joule heating on the flow and heat transfer of an electrically conducting non-Newtonian fluid over to a rotating disk. Turkyilmazoglu and Senel [10] showed the effect of roughness on the heat and mass transfer for the flow past a rotating disk subjected to a wall suction or injection.

Understanding MHD is strongly related to the comprehension of physical effects which take place in MHD. When a conductor moves into a magnetic field, electric current is induced in the conductor and creates its own magnetic field (Lenz's law). Since the induced magnetic field tends to eliminate the original and external supported field, the magnetic field lines will be excluded from the conductor. Conversely, when the magnetic field influences the conductor to move it out of the field, the induced field amplifies the applied

field. The net result of this process is that the lines of force appear to be dragged accompanied by the conductor. In this paper the conductor is the fluid with complex motions. To understand the second key effect which is dynamical we should know that when currents are induced by a motion of a conducting fluid through a magnetic field, a Lorentz force acts on the fluid and modifies its motion. In MHD, the motion modifies the field and vice versa. This makes the theory highly non-linear [11, 12].

HAM is known as one of the most reliable techniques to solve nonlinear problems. HAM was employed by Liao, who was the first, to offer a general analytical method for nonlinear problems [13, 14]. Considering the effects of Brownian motion and thermophoresis, Mustafa *et al* [15] studied stagnation point flow of a nano-fluid towards a stretching sheet using HAM. Rashidi *et al* [16] perused partial slip, thermal-diffusion and diffusion-thermo on MHD flow over a rotating disk with viscous dissipation and Ohmic heating. The mixed convection of an incompressible Maxwell fluid flow over a vertical stretching surface was studied by Abbas *et al* [17] via HAM, considering both cases of assisting and opposing flows. Thermal radiation effect on an exponential stretching surface was perused by Sajid and Hayat [18] via HAM. Rashidi *et al* [19] demonstrated the parametric analysis and optimization of entropy generation in unsteady MHD flow past a stretching rotating disk using artificial neural network (ANN), particle swarm optimization (PSO) algorithm and HAM. Dinarvand *et al* [20] employed HAM to investigate the unsteady laminar (MHD) flow near the forward stagnation point of a rotating and translating sphere. Abbasbandy *et al.* [21] employed HAM for nonlinear boundary value problems. Nowadays HAM has been employed by researchers for different nonlinear problems. Rashidi *et al.* [22] investigated the flow of a viscous incompressible fluid between two parallel plates due to the normal motion of the plates using HAM. In another study, Rashidi *et al* [23] presented the homotopy simulation for nano-fluid dynamics from a non-linearly stretching isothermal permeable sheet with transpiration.

The current perusal is mainly motivated by the need to study the MHD stagnation flow over a porous rotating disk in the presence of the velocity slip condition. HAM, an analytical method, is employed to investigate the effects of physical flow parameters such as magnetic interaction parameter, slip factor, rotation strength parameter, and suction parameter on the fluid velocity in all directions and temperature

distribution.

## 2. Governing equations and mathematical formulation

We consider the 3D steady MHD laminar incompressible flow of electrically conducting viscous fluid over a porous rotating disk in the presence of an externally applied uniform vertical magnetic field in the neighborhood of a stagnation point of a body of revolution. The axisymmetric governing equations for the continuity, momentum and energy in laminar MHD incompressible boundary-layer flow in cylindrical coordinates can be presented, respectively, as follows [24]:

$$\frac{1}{r} \frac{\partial}{\partial r} (ru) + \frac{\partial w}{\partial z} = 0, \quad (1)$$

$$u \frac{\partial u}{\partial r} + w \frac{\partial u}{\partial z} - \frac{v^2}{r} = -\frac{1}{\rho} \frac{\partial p}{\partial r} + \nu \left( \frac{\partial^2 u}{\partial r^2} + \frac{1}{r} \frac{\partial u}{\partial r} + \frac{\partial^2 u}{\partial z^2} - \frac{u}{r^2} \right) + \frac{\sigma B_0^2}{\rho} (u_e - u), \quad (2)$$

$$u \frac{\partial v}{\partial r} + w \frac{\partial v}{\partial z} + \frac{uv}{r} = \nu \left( \frac{\partial^2 v}{\partial r^2} + \frac{1}{r} \frac{\partial v}{\partial r} + \frac{\partial^2 v}{\partial z^2} - \frac{v}{r^2} \right) - \frac{\sigma B_0^2}{\rho} v, \quad (3)$$

$$u \frac{\partial w}{\partial r} + w \frac{\partial w}{\partial z} = -\frac{1}{\rho} \frac{\partial p}{\partial z} + \nu \left( \frac{\partial^2 w}{\partial r^2} + \frac{1}{r} \frac{\partial w}{\partial r} + \frac{\partial^2 w}{\partial z^2} \right), \quad (4)$$

$$u \frac{\partial T}{\partial r} + w \frac{\partial T}{\partial z} = \frac{k}{\rho c_p} \left( \frac{\partial^2 T}{\partial r^2} + \frac{1}{r} \frac{\partial T}{\partial r} + \frac{\partial^2 T}{\partial z^2} \right), \quad (5)$$

where  $\rho$  is the fluid density,  $p$  is the fluid pressure,  $\nu$  is the kinematic viscosity,  $\sigma$  is the electrical conductivity,  $u_e$  is the velocity of the external flow,  $k$  is the thermal conductivity and  $c_p$  is the specific heat at constant pressure. The coordinate system used in this problem is non-rotating cylindrical polar coordinates  $(r, \phi, z)$ . Let the disk rotate with a constant angular velocity  $(\Omega)$  and be placed at  $z = 0$ . The flow velocity components  $(u, v, w)$  are in the directions of increasing cylindrical polar coordinates, respectively. The coordinate system and geometry of the problem are shown in figure 1. An external uniform magnetic field  $B$  is applied normal to the surface of the disk, which has a constant magnetic flux density  $B_0$

that is assumed constant by taking small magnetic Reynolds number much smaller than the fluid Reynolds number. The surface of the rotating disk is maintained at a uniform temperature  $T_w$ , while the temperature and pressure of the ambient fluid are  $T_\infty$  and  $p_\infty$ , respectively. Considering the effect of velocity slip is very important and should be included in the modeling of flow field for the more accurate prediction. In the base of slip flow theory, one can declare that the fluid velocity at the surface is different from the wall velocity compared to the local velocity gradient in normal direction.

The appropriate boundary conditions subject to uniform suction  $w_0$  through the disk and slip condition are introduced as:

$$u = \frac{2-\sigma_v}{\sigma_v} \xi \frac{\partial u}{\partial z}, \quad v = \Omega r + \frac{2-\sigma_v}{\sigma_v} \xi \frac{\partial v}{\partial z}, \quad w = w_0, \quad T = T_w, \quad \text{at} \quad z = 0, \quad (6)$$

$$u \rightarrow u_e, \quad v \rightarrow v_e, \quad T \rightarrow T_\infty, \quad \text{as} \quad z \rightarrow \infty,$$

where  $\sigma_v$  is the tangential momentum accommodation coefficient, which is usually determined empirically [25] and depends on fluid and surface finish,  $\xi$  is the mean free path. It is found that in the potential flow regime:

$$u_e = ar, \quad v_e = 0, \quad w_e = -2az, \quad p = -\frac{1}{2} \rho a^2 (r^2 + 4z^2) + p_0, \quad (7)$$

where  $a$  is a constant and  $p_0$  is the stagnation pressure. Hereupon, the stagnation point occurs at the origin.

The non-dimensional forms of mean flow velocities and temperature distributions of Eqns. (1)-(5) are given by Von Karman's exact self-similar solution of the Navier-Stokes equations:

$$\eta = \sqrt{\frac{a}{\nu}} z, \quad u = ar F(\eta), \quad v = ar G(\eta), \quad w = \sqrt{a\nu} H(\eta), \quad (8)$$

$$p = -\frac{1}{2} \rho a^2 (r^2 + P(\eta)), \quad \theta(\eta) = (T - T_\infty)/(T_w - T_\infty),$$

where  $F$ ,  $G$ ,  $H$  and  $\theta$  are the non-dimensional functions of modified dimensionless vertical coordinate  $\eta$ .

Substituting the above similarity transformations into Eqns. (1)-(5), the nonlinear ordinary differential equations are obtained

$$H'(\eta) + 2F(\eta) = 0, \quad (9)$$

$$F''(\eta) - H(\eta)F'(\eta) - (F(\eta))^2 + (G(\eta))^2 - M(F(\eta) - 1) + 1 = 0, \quad (10)$$

$$G''(\eta) - H(\eta)G'(\eta) - 2F(\eta)G(\eta) - MG(\eta) = 0, \quad (11)$$

$$\frac{1}{Pr}\theta''(\eta) - H(\eta)\theta'(\eta) = 0, \quad (12)$$

where  $M = \sigma B_0^2 / \rho a$  is the magnetic interaction parameter,  $Pr = \mu c_p / k$  is the Prandtl number and primes denote differentiation with respect to  $\eta$ . The transformed boundary conditions become

$$\begin{aligned} F(0) &= \gamma F'(0), & G(0) &= \omega + \gamma G'(0), & H(0) &= W_s, & \theta(0) &= 1, \\ F(\eta) &\rightarrow 1, & G(\eta) &\rightarrow 0, & \theta(\eta) &\rightarrow 0, & \text{as } \eta &\rightarrow \infty, \end{aligned} \quad (13)$$

where  $\gamma = [(2 - \sigma_v)\xi\sqrt{a/\nu}] / \sigma_v$  is the slip factor,  $\omega = \Omega/a$  shows a rotation strength parameter,

$W_s = w_0 / (a\nu)^{1/2}$  is the suction/injection parameter and  $W_s < 0$  corresponds to a uniform suction at the disk surface.

### 3. HAM solution

We choose the appropriate initial approximations, to satisfy the above boundary conditions, as follows:

$$H_0(\eta) = W_s, \quad (14)$$

$$F_0(\eta) = 1 - \frac{e^{-\eta}}{\gamma + 1}, \quad (15)$$

$$G_0(\eta) = \frac{\omega}{\gamma + 1} e^{-\eta}, \quad (16)$$

$$\theta_0(\eta) = e^{-\eta}, \quad (17)$$

The linear operators  $L_H(H)$ ,  $L_F(F)$ ,  $L_G(G)$ , and  $L_\theta(\theta)$  are introduced as:

$$L_H(H) = \frac{\partial H}{\partial \eta}, \quad (18)$$

$$L_F(F) = \frac{\partial^2 F}{\partial \eta^2} + \frac{\partial F}{\partial \eta}, \quad (19)$$

$$L_G(G) = \frac{\partial^2 G}{\partial \eta^2} + \frac{\partial G}{\partial \eta}, \quad (20)$$

$$L_\theta(\theta) = \frac{\partial^2 \theta}{\partial \eta^2} + \frac{\partial \theta}{\partial \eta}, \quad (21)$$

with the following properties:

$$L_H(c_1) = 0, \quad (22)$$

$$L_F(c_2 e^{-\eta} + c_3) = 0, \quad (23)$$

$$L_G(c_4 e^{-\eta} + c_5) = 0, \quad (24)$$

$$L_\theta(c_6 e^{-\eta} + c_7) = 0, \quad (25)$$

where  $c_i, i=1-7$  are the arbitrary constants. According to Eqns. (9)-(12), the nonlinear operators are defined as

$$N_H[\hat{H}(\eta; q), \hat{F}(\eta; q)] = \frac{\partial \hat{H}(\eta; q)}{\partial \eta} + 2\hat{F}(\eta; q), \quad (26)$$

$$N_F[\hat{H}(\eta; q), \hat{F}(\eta; q), \hat{G}(\eta; q)] = \frac{\partial^2 \hat{F}(\eta; q)}{\partial \eta^2} - \hat{H}(\eta; q) \frac{\partial \hat{F}(\eta; q)}{\partial \eta} - \hat{F}(\eta; q)^2 + \hat{G}(\eta; q)^2 - M(\hat{F}(\eta; q) - 1) + 1, \quad (27)$$

$$N_G[\hat{H}(\eta; q), \hat{F}(\eta; q), \hat{G}(\eta; q)] = \frac{\partial^2 \hat{G}(\eta; q)}{\partial \eta^2} - \hat{H}(\eta; q) \frac{\partial \hat{G}(\eta; q)}{\partial \eta} - 2\hat{G}(\eta; q)\hat{F}(\eta; q) - M\hat{G}(\eta; q), \quad (28)$$

$$N_\theta[\hat{H}(\eta; q), \hat{\theta}(\eta; q)] = \frac{1}{Pr} \frac{\partial^2 \hat{\theta}(\eta; q)}{\partial \eta^2} - \hat{H}(\eta; q) \frac{\partial \hat{\theta}(\eta; q)}{\partial \eta}, \quad (29)$$

The auxiliary functions become:

$$H_H(\eta) = 1, \quad H_F(\eta) = H_G(\eta) = H_\theta(\eta) = e^{-\eta}, \quad (30)$$

The symbolic software *MATHEMATICA* is employed to solve the  $m$ th order deformation equations (31)-

(34).

$$\mathcal{L}_H \left[ H_m(\eta) - \chi_m H_{m-1}(\eta) \right] = \hbar H_H(\eta) R_{H,m}(\eta), \quad (31)$$

$$\mathcal{L}_F \left[ F_m(\eta) - \chi_m F_{m-1}(\eta) \right] = \hbar H_F(\eta) R_{F,m}(\eta), \quad (32)$$

$$\mathcal{L}_G \left[ G_m(\eta) - \chi_m G_{m-1}(\eta) \right] = \hbar H_G(\eta) R_{G,m}(\eta), \quad (33)$$

$$\mathcal{L}_\theta \left[ \theta_m(\eta) - \chi_m \theta_{m-1}(\eta) \right] = \hbar H_\theta(\eta) R_{\theta,m}(\eta), \quad (34)$$

where  $\hbar$  is the auxiliary nonzero parameter and

$$R_{H,m}(\eta) = \frac{\partial H_{m-1}(\eta)}{\partial \eta} + 2F_{m-1}(\eta), \quad (35)$$

$$R_{F,m}(\eta) = \frac{\partial^2 F_{m-1}(\eta)}{\partial \eta^2} - \sum_{n=0}^{m-1} \left( H_n(\eta) \frac{\partial F_{m-1-n}(\eta)}{\partial \eta} + F_n(\eta) F_{m-1-n}(\eta) - G_n(\eta) G_{m-1-n}(\eta) \right) - M (F_{m-1}(\eta) - 1) + 1, \quad (36)$$

$$R_{G,m}(\eta) = \frac{\partial^2 G_{m-1}(\eta)}{\partial \eta^2} - \sum_{n=0}^{m-1} \left( H_n(\eta) \frac{\partial G_{m-1-n}(\eta)}{\partial \eta} + 2F_n(\eta) G_{m-1-n}(\eta) \right) - M G_{m-1}(\eta), \quad (37)$$

$$R_{\theta,m}(\eta) = \frac{1}{Pr} \frac{\partial^2 \theta_{m-1}(\eta)}{\partial \eta^2} - \sum_{n=0}^{m-1} \left( H_n(\eta) \frac{\partial \theta_{m-1-n}(\eta)}{\partial \eta} \right), \quad (38)$$

and

$$\chi_m = \begin{cases} 0, & m \leq 1, \\ 1, & m > 1, \end{cases} \quad (39)$$

are the involved parameters in HAM theory. See Ref [13, 26, 27], for more information about the different steps of HAM. It is important to choose a proper value of auxiliary parameter to control and speed the convergence of the approximation series by the help of the so-called  $\hbar$  – curve. Obviously, the valid regions of  $\hbar$  correspond to the line segments nearly parallel to the horizontal axis. The  $\hbar$ –curves of  $F'(0)$ ,  $G'(0)$ ,  $H'''(0)$ , and  $\theta'(0)$  obtained by the 20<sup>th</sup> order of HAM solution are shown in Fig. 2. a.

In order to acquire the optimal values of auxiliary parameters, the averaged residual errors are defined as:

$$Res_H = \frac{dH(\eta)}{d\eta} + 2F(\eta), \quad (40)$$

$$Res_F = \frac{d^2F(\eta)}{d\eta^2} - H(\eta) \frac{dF(\eta)}{d\eta} - F(\eta)^2 + G(\eta)^2 - M(F(\eta) - 1) + 1, \quad (41)$$

$$Res_G = \frac{d^2G(\eta)}{d\eta^2} - H(\eta) \frac{dG(\eta)}{d\eta} - 2F(\eta)G(\eta) - M G(\eta), \quad (42)$$

$$Res_\theta = \frac{1}{Pr} \frac{d^2\theta(\eta)}{d\eta^2} - H(\eta) \frac{d\theta(\eta)}{d\eta}, \quad (43)$$

The residual errors for 20<sup>th</sup> order of HAM solutions of Eq. (41) are illustrated in Fig. 2. b, to survey the accuracy of the present method.

#### 4. Results and Discussion

The nonlinear ordinary differential equations (9)-(12) subject to the boundary conditions (13) have been solved via HAM for some values of the magnetic interaction parameter ( $M$ ), slip factor ( $\gamma$ ), rotation strength parameter ( $\omega$ ), and suction parameter ( $W_s$ ). For the present investigation, the value of the Prandtl number ( $Pr$ ) is considered equal to 0.71. The values of the flow physical parameters are mentioned in each of the graphs and tables. Table 1 illustrates a comparison between the presented results and those reported by Turkyilmazoglu [24] for  $F'(0)$  and  $G'(0)$  and different value of the magnetic interaction parameter. An excellent agreement can be observed between them. Tables 2-4 depict numerical values of the skin friction coefficients and rate of heat transfer for different values of the suction parameter and slip factor.

Figure 3 represents the influence of magnetic interaction parameter on the radial, tangential and axial velocity components as well as temperature distribution. A drag-like Lorentz force is created by the inflection of the vertical magnetic field on the electrically conducting fluid. This drag-like force has tendency to slow down the flow around the disk. Therefore, all velocity **boundary layer thicknesses** decrease, as the magnetic field gets stronger. It is worth mentioning that the large resistances on the fluid particles apply as the vertical

magnetic field increases.

The effect of slip parameter on the velocity components and temperature distribution is demonstrated in figure 4. In the presence of the slip condition, the radial velocity boundary layer thickness reduces. In addition, the radial velocity profile starts from zero only in the no slip condition cases. The fluid velocity **boundary layer thicknesses** in radial, tangential and axial directions decrease with increasing the values of the slip factor. In other word, the less amount of flow is drawn and pushed away in the velocity directions, as the slip gets stronger. It is also observed that the value of the temperature component reduces as the slip parameter increases.

Figure 5 illustrates the effect of rotation strength parameter on the radial, tangential and axial velocity components and the thermal boundary-layer thickness. As the rotation strength parameter increases, the velocity profiles in tangential direction increases and the radial velocity boundary layer thickness, the axial velocity component and thermal boundary-layer thickness reduce. It is worth mentioning that as the rotation parameter increases the centrifugal force pokes the fluid particles in the radial direction. The enhancement in the rotation strength parameters leads to reduce the axial velocity component, whose decrease is due to the reason that increasing rotation augments the pumping of fluid particles in the radial direction.

Figure 6 shows the effect of suction parameter on all velocity components and the temperature distribution. Applying suction at the disk surface causes to reduce all the fluid velocity profiles. This phenomenon happens because of this fact that applying suction leads to draw the amount of fluid particles into the wall and consequently the velocity boundary-layers decrease. In addition, the usual decay of temperature distribution occurs for larger values of the suction parameter.

Figures 7-a&b present the velocity contours in radial and axial directions. As the radial coordinate increases, the primitive radial ( $u$ ) velocity component increases. This velocity component is maximized near the surface of the disk i.e. at low values of axial coordinate (bottom right hand corner of Figure 7-a). From Figure 7-b, it is obvious that the axial velocity component is maximized near the disk surface for all values of radial coordinate. As we depart from the surface, the axial velocity component decays. In order to have a

better grasp of the fluid flow, the velocity vectors are shown in figure 7-c. Fluid is clearly drawn in a fan like mechanism outwards along the radial coordinate and in the negative axial direction. This template characterizes the Von Karman swirling flow [1].

## **5. Conclusions**

In the current study, a mathematical formulation has been derived for an MHD stagnation flow due to a porous rotating disk in the presence of the velocity slip. HAM is used to solve the system of ordinary differential equations. The present semi numerical/analytical simulations agree closely with the previous studies for some especial cases. HAM has been shown to be a very strong and efficient technique in finding analytical solutions for nonlinear differential equations. The effects of the five key thermo-physical parameters governing the flow i.e. magnetic interaction parameter, slip factor, rotation strength parameter, and suction parameter on the all dimensionless velocity components and temperature distributions as well as skin friction coefficient and local Nusselt number have been presented graphically and interpreted in details. These computations have provided some further insights into the fluid mechanics and thermodynamics of proposed rotating disk MHD systems coupled with nuclear space propulsion engines.

## References

- [1] T. V. Kármán, Über laminare und turbulente Reibung, *ZAMM - Journal of Applied Mathematics and Mechanics / Zeitschrift für Angewandte Mathematik und Mechanik* 1 (1921) 233-252.
- [2] I. V. Shevchuk, M. H. Buschmann, Rotating disk heat transfer in a fluid swirling as a forced vortex, *Heat and Mass Transfer* 41 (2005) 1112-1121.
- [3] H. A. Attia, Steady Flow over a Rotating Disk in Porous Medium with Heat Transfer, *Nonlinear Analysis: Modelling and Control* 14 (2009) 21–26.
- [4] E. Osalusi, J. Side, R. Harris, The effects of Ohmic heating and viscous dissipation on unsteady MHD and slip flow over a porous rotating disk with variable properties in the presence of Hall and ion-slip currents, *International Communications in Heat and Mass Transfer* 34 (2007) 1017-1029.
- [5] I. V. Shevchuk, *Convective Heat and Mass Transfer in Rotating Disk Systems*, Springer, 2009.
- [6] S. Asghar, M. Jalil, M. Hussan, M. Turkyilmazoglu, Lie group analysis of flow and heat transfer over a stretching rotating disk, *International Journal of Heat and Mass Transfer* 69 (2014) 140-146.
- [7] C. Y. Wang, Flow due to a stretching boundary with partial slip—an exact solution of the Navier–Stokes equations, *Chemical Engineering Science* 57 (2002) 3745-3747.
- [8] E. M. Sparrow, G. S. Beavers, L. Y. Hung, Flow about a porous-surfaced rotating disk, *International Journal of Heat and Mass Transfer* 14 (1971) 993-996.
- [9] B. Sahoo, Effects of partial slip, viscous dissipation and Joule heating on Von Kármán flow and heat transfer of an electrically conducting non-Newtonian fluid, *Communications in Nonlinear Science and Numerical Simulation* 14 (2009) 2982-2998.
- [10] M. Turkyilmazoglu, P. Senel, Heat and mass transfer of the flow due to a rotating rough and porous disk, *International Journal of Thermal Sciences* 63 (2013) 146-158.
- [11] P. A. Davidson, *An introduction to magnetohydrodynamics*, Cambridge University Press, 2001.
- [12] M. M. Rashidi, B. Rostami, N. Freidoonimehr, S. Abbasbandy, Free convective heat and mass transfer for MHD fluid flow over a permeable vertical stretching sheet in the presence of the radiation and buoyancy effects, *Ain Shams Engineering Journal* 5 (2014) 901–912.
- [13] S. J. Liao, *Beyond perturbation: introduction to the homotopy analysis method*, Chapman & Hall/CRC, 2004.
- [14] S. J. Liao, On the homotopy analysis method for nonlinear problems, *Appl. Math. Comput.* 147 (2004) 499-513.
- [15] M. Mustafa, T. Hayat, I. Pop, S. Asghar, S. Obaidat, Stagnation-point flow of a nanofluid towards a stretching sheet, *International Journal of Heat and Mass Transfer* 54 (2011) 5588-5594.
- [16] M. M. Rashidi, T. Hayat, E. Erfani, S. A. Mohimani Pour, A. A. Hendi, Simultaneous effects of partial slip and thermal-diffusion and diffusion-thermo on steady MHD convective flow due to a rotating disk, *Commun Nonlinear Sci Numer Simulat* 16 (2011) 4303-4317.
- [17] Z. Abbas, Y. Wang, T. Hayat, M. Oberlack, Mixed convection in the stagnation-point flow of a Maxwell fluid towards a vertical stretching surface, *Nonlinear Analysis: Real World Applications* 11 (2010) 3218-3228.
- [18] M. Sajid, T. Hayat, Influence of thermal radiation on the boundary layer flow due to an exponentially stretching sheet, *International Communications in Heat and Mass Transfer* 35 (2008) 347-356.
- [19] M. M. Rashidi, M. Ali, N. Freidoonimehr, F. Nazari, Parametric analysis and optimization of entropy generation in unsteady MHD flow over a stretching rotating disk using artificial neural network and particle swarm optimization algorithm, *Energy* (2013).
- [20] S. Dinarvand, A. Doosthoseini, E. Doosthoseini, M. M. Rashidi, Series solutions for unsteady laminar MHD flow near forward stagnation point of an impulsively rotating and translating sphere in presence of buoyancy forces, *Nonlinear Analysis: Real World Applications* 11 (2010) 1159-1169.
- [21] S. Abbasbandy, E. Magyari, E. Shivanian, The homotopy analysis method for multiple solutions of

- nonlinear boundary value problems, *Communications in Nonlinear Science and Numerical Simulation* 14 (2009) 3530-3536.
- [22] M. M. Rashidi, H. Shahmohamadi, S. Dinarvand, Analytic Approximate Solutions for Unsteady Two-Dimensional and Axisymmetric Squeezing Flows between Parallel Plates, *Mathematical Problems in Engineering* 2008 (2008).
- [23] M. M. Rashidi, N. Freidoonimehr, A. Hosseini, O. A. Bég, T. K. Hung, Homotopy simulation of nanofluid dynamics from a non-linearly stretching isothermal permeable sheet with transpiration, *Meccanica* (2013) 1-14.
- [24] M. Turkyilmazoglu, Three dimensional MHD stagnation flow due to a stretchable rotating disk, *International Journal of Heat and Mass Transfer* 55 (2012) 6959-6965.
- [25] M. Renksizbulut, H. Niazmand, G. Tercan, Slip-flow and heat transfer in rectangular microchannels with constant wall temperature, *International Journal of Thermal Sciences* 45 (2006) 870-881.
- [26] S. J. Liao, An explicit, totally analytic approximation of Blasius viscous flow problems, *International Journal of Non-Linear Mechanics* 34 (1999) 759-778.
- [27] M. M. Rashidi, S. A. Mohimani Pour, S. Abbasbandy, Analytic approximate solutions for heat transfer of a micropolar fluid through a porous medium with radiation, *Communications in Nonlinear Science and Numerical Simulation* 16 (2011) 1874-1889.

## Figures

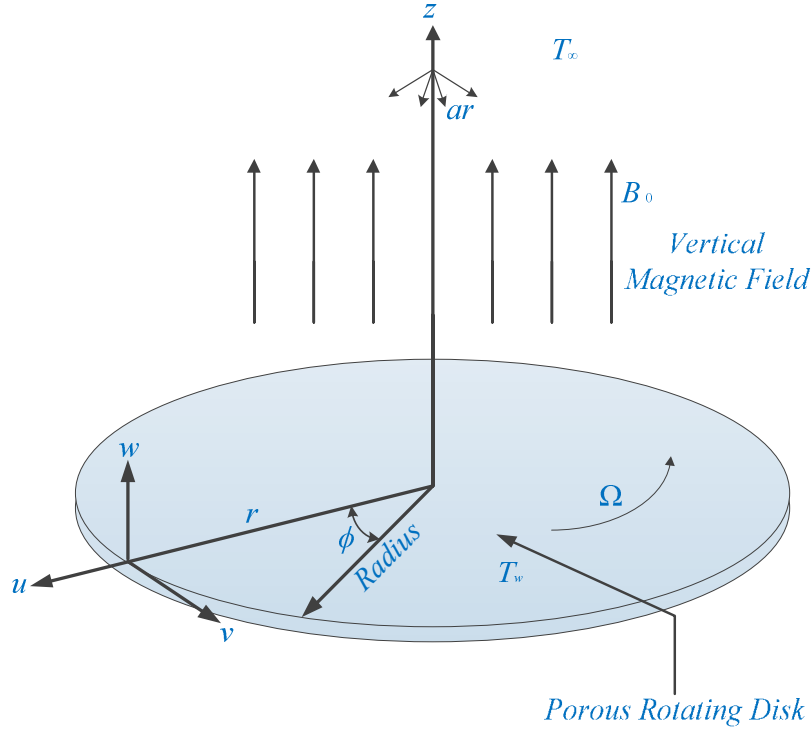


Figure 1: Schematic of the flow configuration and geometrical coordinates.

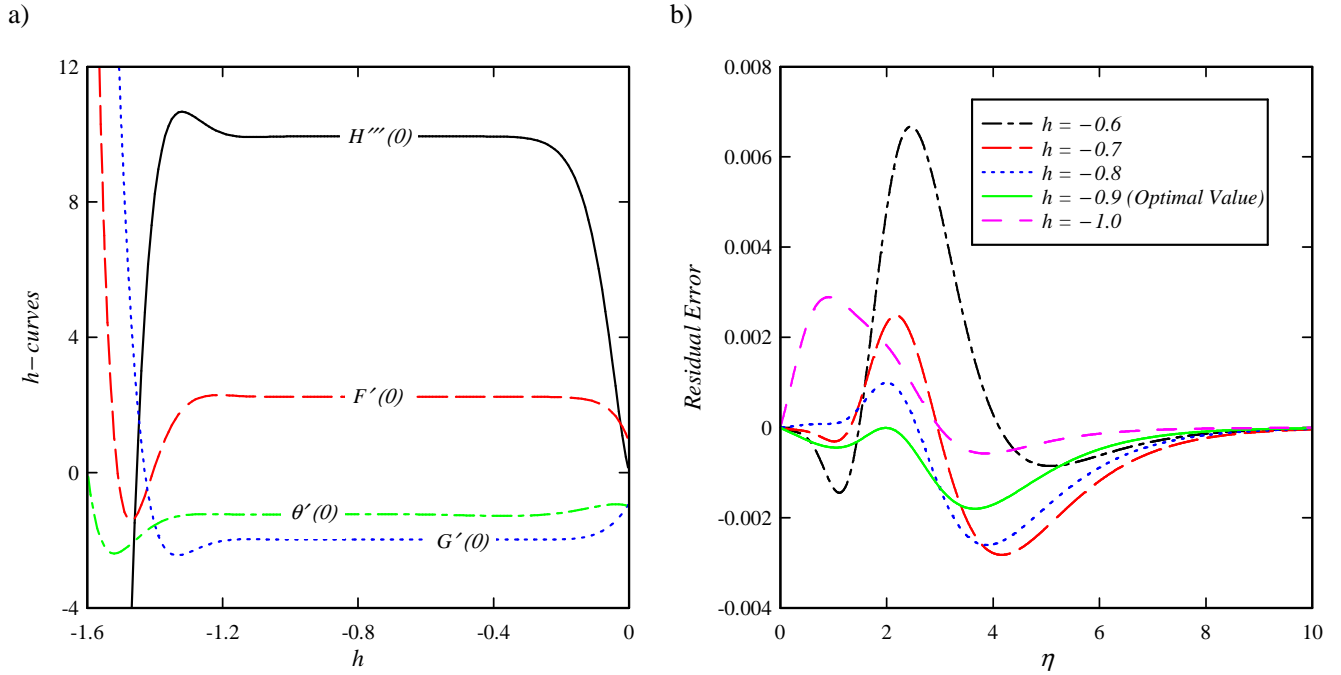


Figure 2: a) The  $h$  - curves of  $H'''(0)$ ,  $F'(0)$ ,  $G'(0)$  and  $\theta'(0)$  and b) The residual error of Eq. (41) obtained by the 20<sup>th</sup> order approximation of the HAM solution when  $M = \omega = -W_s = 1$  and  $\gamma = 0.1$ .

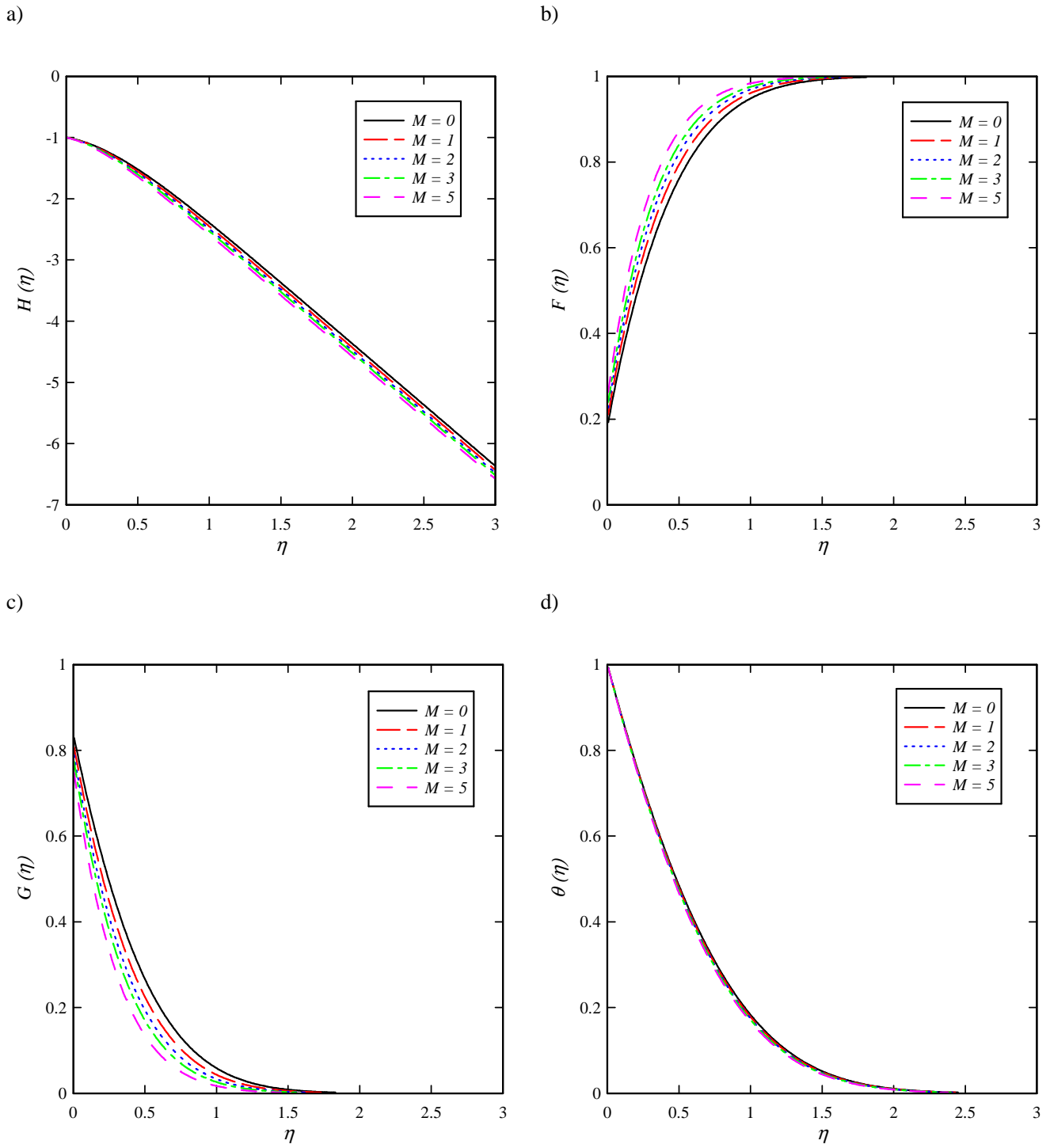


Figure 3: Effect of magnetic interaction parameter on a) axial b) radial c) tangential velocity components and d) temperature distribution when  $\omega=1$ ,  $W_s = -1$  and  $\gamma=0.1$ .

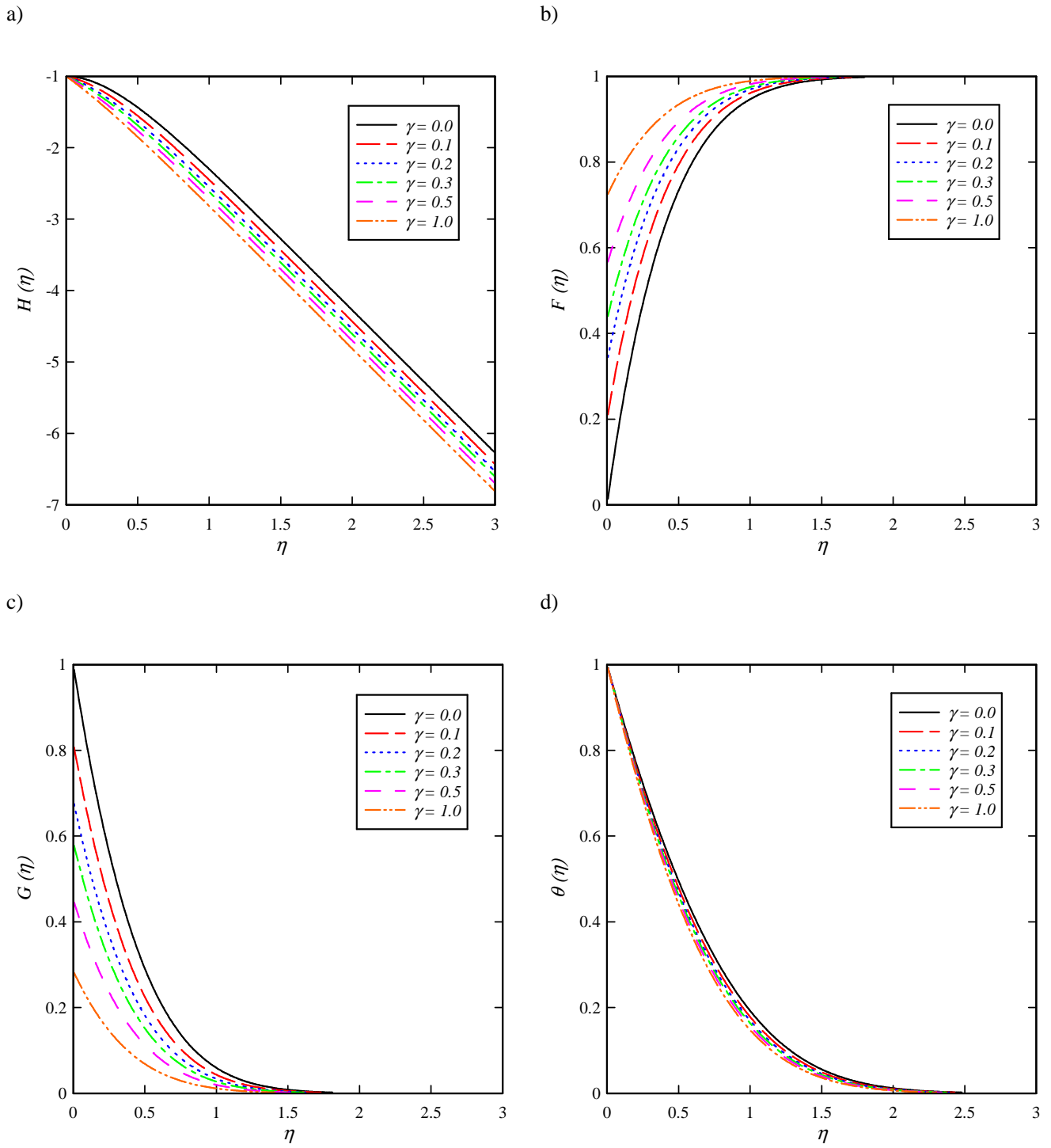


Figure 4: Effect of slip parameter on a) axial b) radial c) tangential velocity components and d) temperature distribution when  $M = \omega = 1$  and  $W_s = -1$ .

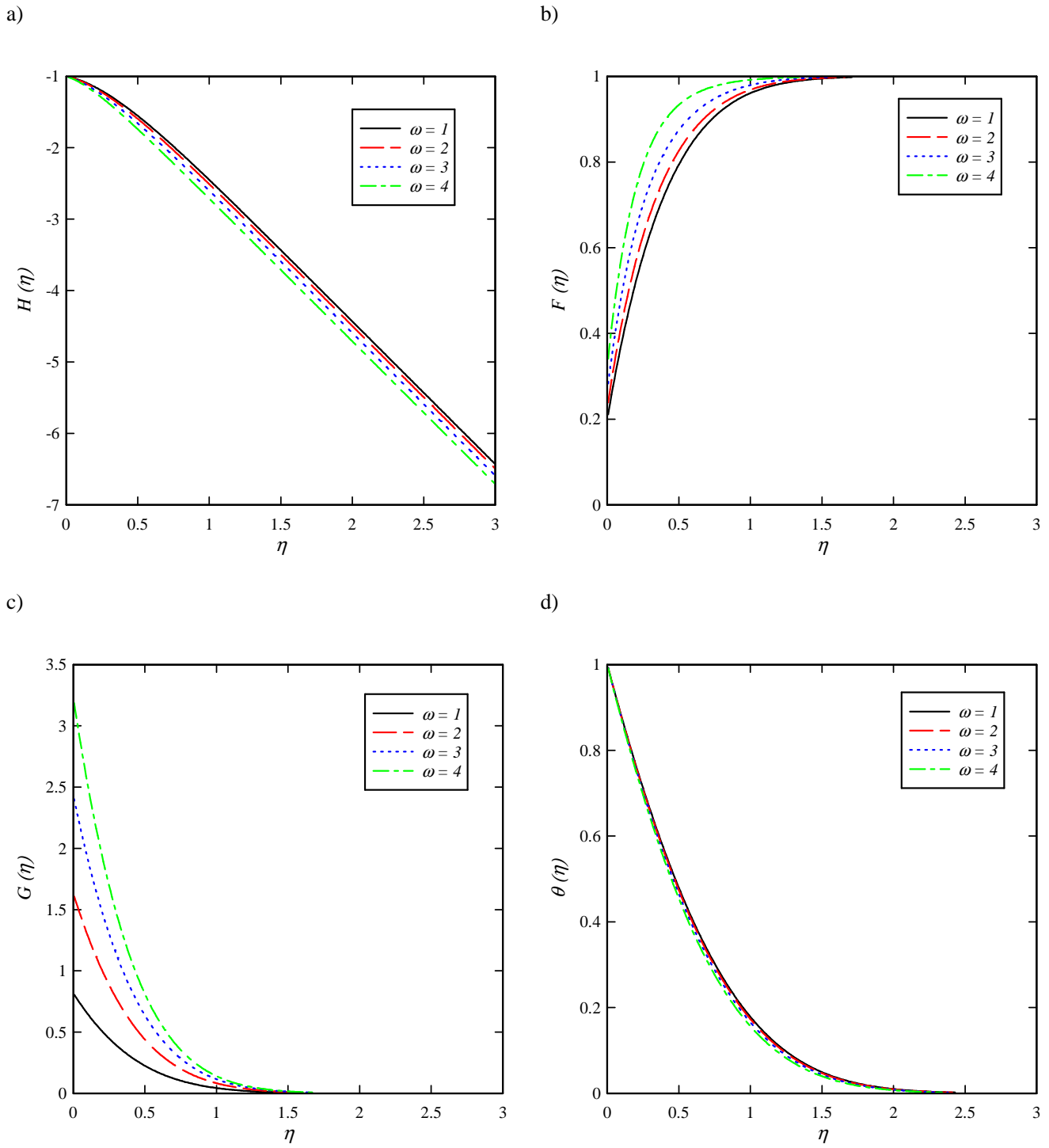


Figure 5: Effect of rotation strength parameter on a) axial b) radial c) tangential velocity components and d) temperature distribution when  $M = 1$ ,  $W_s = -1$  and  $\gamma = 0.1$ .

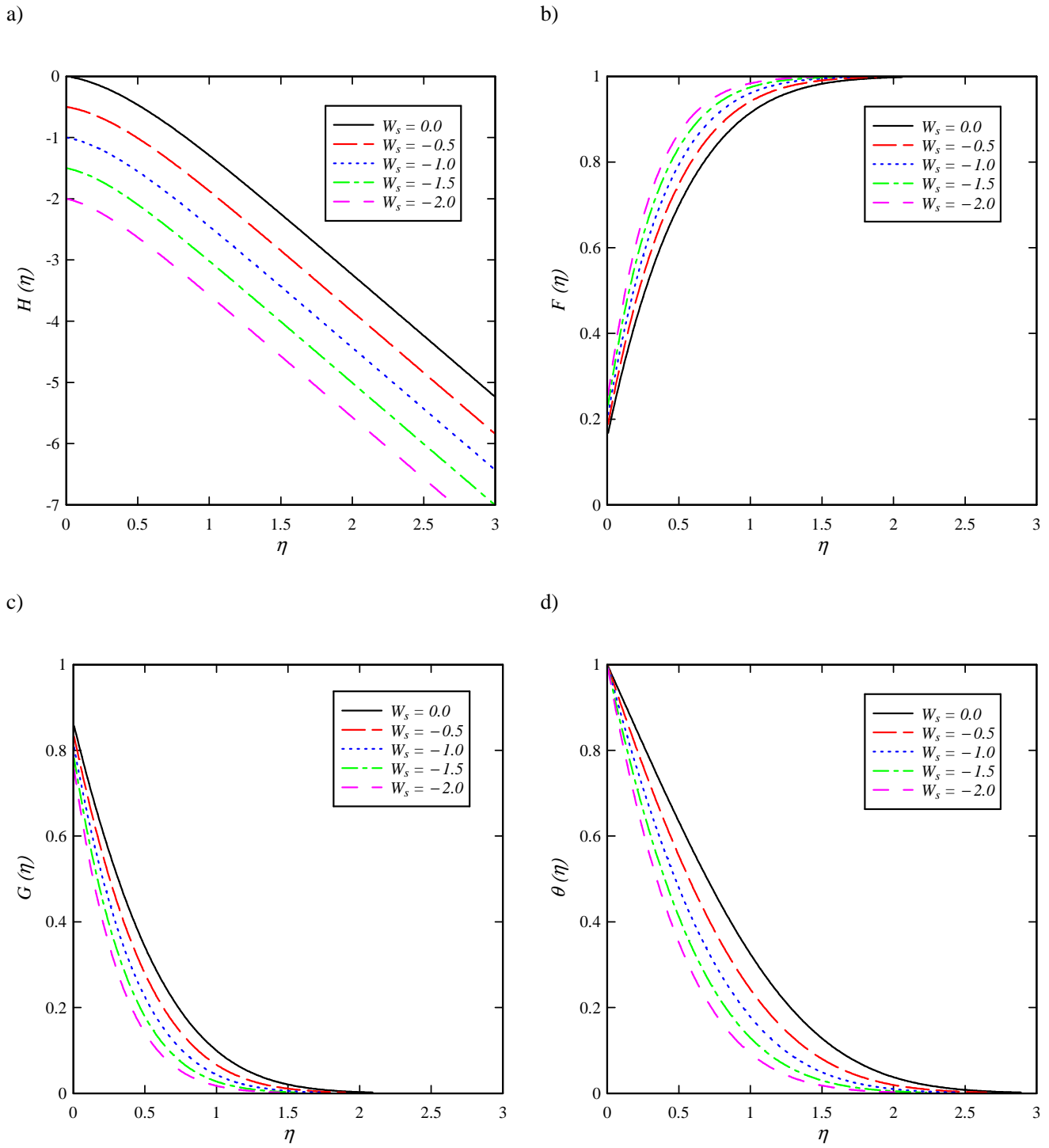


Figure 6: Effect of suction parameter on a) axial b) radial c) tangential velocity components and d) temperature distribution when  $M = \omega = 1$  and  $\gamma = 0.1$ .

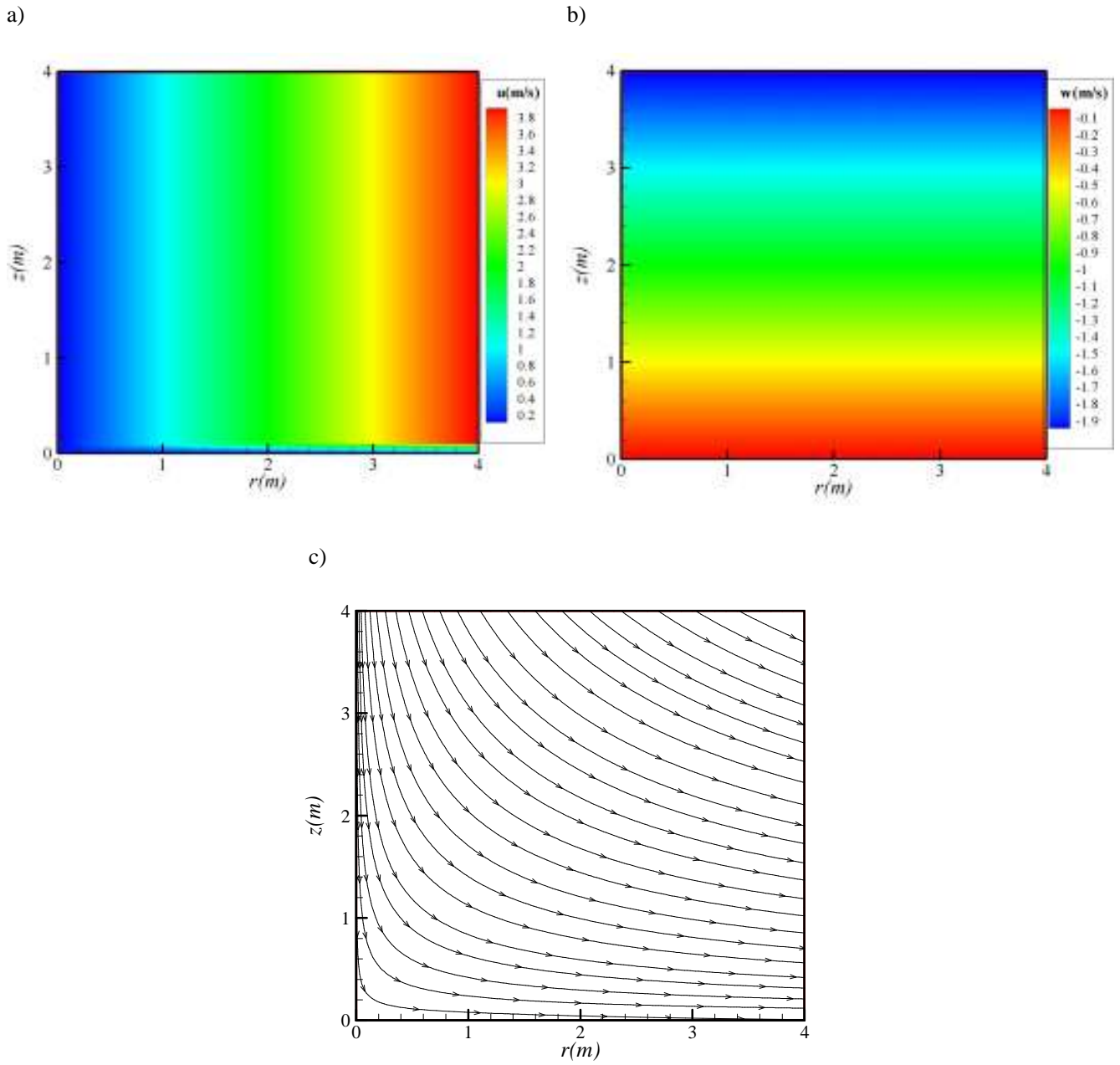


Figure 7: a) Radial velocity contour b) Axial velocity contour and c) Vector analysis with the vector variables of  $u$  and  $w$  when  $M = \omega = -W_s = a = 1$ ,  $\gamma = 0.1$  and  $\nu = 1.5 \times 10^{-5} \text{ (m}^2/\text{s)}$ .

## Tables

**Table 1:**

Comparison between the results of present study with the results reported by Turkyilmazoglu [24] for  $F'(0)$  and  $-G'(0)$  and different values of the magnetic interaction parameter when  $\omega = 2$  and  $W_s = \gamma = 0$ .

$M$	$F'(0)$		$-G'(0)$	
	Present	Ref. [23]	Present	Ref. [23]
0	2.295642283711	2.2956422869	2.393661963184	2.3936619498
1	2.453325131091	2.4533251351	3.041585272826	3.0415852559
2	2.620862841949	2.6208628461	3.601362344177	3.6013623342
5	3.106851835286	3.1068518380	4.956835245622	4.9568352387

**Table 2:**

Numerical values of the radial skin friction coefficient ( $F'(0)$ ) for different values of the suction parameter ( $W_s$ ) and slip factor ( $\gamma$ ) when  $M = \omega = 1$ .

$W_s$	$\gamma = 0$	$\gamma = 0.5$	$\gamma = 1$
0	1.85378891	0.98591725	0.66338194
-1	2.45041073	1.12259375	0.72122532
-2	3.15845036	1.24170373	0.76749355
-3	3.94772094	1.34041906	0.80340936

**Table 3:**

Numerical values of the tangential skin friction coefficient  $(-G'(0))$  for different values of the suction parameter  $(W_s)$  and slip factor  $(\gamma)$  when  $M = \omega = 1$ .

$W_s$	$\gamma = 0$	$\gamma = 0.5$	$\gamma = 1$
0	1.47013629	0.93615979	0.64949106
-1	2.12505924	1.09603405	0.71466016
-2	2.88698318	1.22751493	0.76430872
-3	3.72025303	1.33258491	0.80178116

**Table 4:**

Numerical values of the heat transfer rate  $(-\theta'(0))$  for different values of the suction parameter  $(W_s)$  and slip factor  $(\gamma)$  when  $M = \omega = 1$ .

$W_s$	$\gamma = 0$	$\gamma = 0.5$	$\gamma = 1$
0	0.70526567	0.83129079	0.87249549
-1	1.21486195	1.34816468	1.38390410
-2	1.80074808	1.92938227	1.95818403
-3	2.43044518	2.54972643	2.57242006